IOP Conference Series: Earth and Environmental Science

PAPER • **OPEN ACCESS**

Characterization of no-load conditions for a high head Francis turbine based on the swirl level

To cite this article: M Fortin *et al* 2022 *IOP Conf. Ser.: Earth Environ. Sci.* **1079** 012010

View the article online for updates and enhancements.

Characterization of no-load conditions for a high head Francis turbine based on the swirl level

M Fortin[1], B Nennemann[2] and S Houde[1],

[1] LAMH, Mechanical Engineering Department, 1065 avenue de la médecine, Université Laval, Québec G1V 0A6, Canada
[2] Andritz Hydro Canada Inc., 6100 Transcanada Highway, Pointe-Claire, Québec H9R 1B9, Canada

E-mail: melissa.fortin.2@ulaval.ca

Abstract. This paper compares the average flow topology in the draft tube cone of a high head Francis turbine operated at full-gate opening no-load (runaway) and speed-no-load (SNL). The comparison is based on the swirl level in the turbine quantified with the angular momentum parameter (RC_{u11}) and the Swirl number. This study shows that RC_{u11} only depends on the flow angle at the guide vane outlet, the distributor height and the runner outlet diameter. The Swirl number has strong limitations in characterizing the flow at runaway and SNL and is unsuitable for no-load conditions.

1. Introduction

No-load (NL) are operating conditions where the turbine produces zero net torque, i.e., the mechanical torque produced by the runner is equal to the friction losses. Different NL conditions are known to have different flow topologies [1]. The speed-no-load (SNL) is a NL condition reached at small guide vane openings where the turbine rotates at the generator synchronous speed. For this NL condition, a large backflow is present in the draft tube cone, which extends into the runner interblade channels [2], [3]. Another well-known NL condition is the runaway, where the guide vanes are fully open and the runner is free to reach a high rotation speed. From SNL to runaway, the backflow size in the draft tube cone decreases as the guide vanes open [1], [4], [5]. At some point, the backflow no longer enters the runner [1], [6]. The flow topology in the draft tube becomes similar to the one at part load operation [1].

The swirl level is used to qualify the flow topology or the flow instabilities in the turbine at different operating conditions [7]–[9]. A swirling flow has a non-zero circumferential velocity component and an axial velocity component. The main objective of this paper is to link the average runaway and SNL operating points and their flow topology in the draft tube cone to the swirl level via the angular momentum parameter and the Swirl number. The parameters driving the swirl level in the turbine and the effect of the runner in a hydraulic channel under a given swirl level are identified. Finally, this paper compares the ability of the angular momentum parameter and the Swirl number to characterize NL conditions. The study is based on Unsteady Reynolds-Averaged Navier-Stokes (URANS) simulations of a model Francis turbine.

2. Swirl definitions

2.1 Angular momentum parameter - RC_{u11}

RC_{u11} is the axial flux of angular momentum normalized by the discharge squared in a dimensionless expression. This swirl definition was used to characterize the draft tube surge

[10], [11] and, more recently, to qualify NL conditions [1], [12]. RC_{u11} is derived from the angular momentum equation put in the form of the Euler turbine equation:

$$M_1\text{-}M_2=T_{Eu} \tag{1}$$

In equation (1), T_{Eu} [Nm] is the hydraulic torque or the Euler torque and M [Nm] is the moment defined as follows:

$$M_1=\int_0^A(r\cdot C_u)\cdot\rho\cdot\vec{C}\cdot(-\vec{n})dA,\ \ M_2=\int_0^A(r\cdot C_u)\cdot\rho\cdot\vec{C}\cdot\vec{n}dA. \tag{2}$$

In equation (2), r [m] is the radius coordinate, C_u [m/s] the circumferential velocity component, ρ [kg/m^3] is the fluid density, $\vec{C}$ [m/s] is the velocity vector, $\vec{n}$ is the unit vector normal to a section and A [m^2] the area of a section. The locations of the runner inlet (1) and outlet (2) on a meridional contour of a Francis turbine are shown in figure 1. Since the transient term in the angular momentum equation has been neglected, equation (1) is only valid at steady operating conditions.

The dimensionless form of equation (1) is:

$$(RC_{u11})_1\text{-}(RC_{u11})_2=\frac{T_{Eu}D_2}{\rho Q^2}, \tag{3}$$

where RC_{u11} is the angular momentum parameter and $\frac{T_{Eu}D_2}{\rho Q^2}$ is the Euler torque parameter. In the Euler torque parameter, D_2 [m] is the runner outlet diameter and Q [m^3/s] the discharge. The angular momentum parameter is defined as follows:

$$(RC_{u11})_i=\frac{D_2M_i}{\rho Q^2}, \tag{4}$$

where i is 1 at the runner inlet and 2 at the runner outlet.

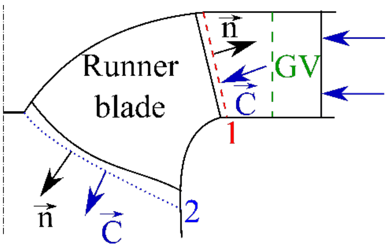

Figure 1. Meridional contour of a Francis turbine showing the guide vane (GV) outlet, the runner inlet (index 1) and the runner outlet (index 2) positions.

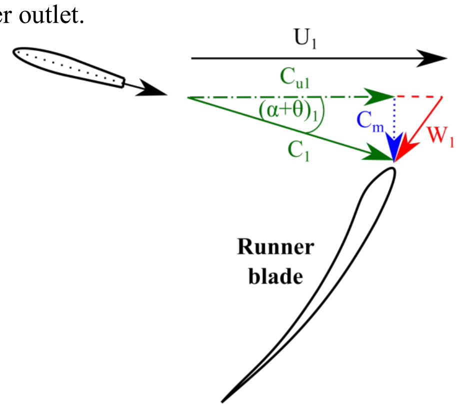

Figure 2. Theoretical velocity triangles at the guide vane outlet and the runner inlet.

As presented in Fortin et al. [1], for an incompressible flow, the analytical definition of RC_{u11} at the runner inlet is

$$(RC_{u11})_1=\frac{1}{2\pi}\cdot\frac{D_2}{B_0}\cdot\frac{1}{\tan(\alpha+\theta)}, \tag{5}$$

where (α+θ) [°] is the average flow angle on a plane at a short distance downstream of the guide vane trailing edges and B_0 [m] the distributor height. Figure 2 shows (α+θ) on the velocity triangles at the guide vane outlet and the runner inlet. The component α [°] of the flow angle is the guide vane opening and the component θ [°], the flow correction angle, represents the deviation between the flow angle and α, caused in part by the guide vane profile (e.g., asymmetrical or symmetrical).

2.2 Swirl number

The Swirl number S is the most commonly used parameter in hydraulic turbines to quantify the swirl at the runner outlet or in the draft tube cone [9], [13]. The Swirl number is defined by

$$S=\frac{M}{(D_2/2)\cdot F_a}, \tag{6}$$

where M and F_a [N] are the moment and the axial force on a plane under the runner. The moment has the same definition as M_2 in equation (2). According to the linear momentum equation, the axial force on a plane is

$$F_a=\int_0^A C_a\rho(\vec{C}\cdot\vec{n})dA\,. \tag{7}$$

A pressure term is usually included in the axial force definition to consider the axial thrust [14], [15]. This term is neglected here, as in most studies in hydraulic turbines [9], [13], since the definition of a pressure term relevant in the hydraulic turbine field needs more investigations. Also, Gupta et al. [14] and Vignat et al. [15] showed that the average Swirl number value is composed of average terms, linked to the average velocity components, and fluctuating terms, also called turbulent stress terms. In this paper, the average Swirl number and RC_{u11} values are always calculated with the average and fluctuating terms. However, it has to be kept in mind that fluctuations engendered by the turbulence are modeled in the simulations.

The runner outlet diameter in equation (6) is used as a reference diameter. In hydraulic turbines, the reference diameter in the Swirl number definition is often the maximum diameter of the plane where the swirl is calculated. This Swirl number definition comes from analyses in furnaces [14], where the furnace diameter affects the size and the shape of the vortex breakdown, not only the diameter of the nozzle injecting the swirling flow. In a draft tube cone, the maximum diameter of a plane changes with its axial position. Using a reference diameter changing with the plane location induces a variation of the Swirl number not based on fluid mechanics laws. For this reason, in this paper, the Swirl number is evaluated with equation (6) using D_2 as reference diameter, whatever the location where the swirl is calculated.

3. Test case: High head Francis turbine and investigated no-load conditions

The numerical studies at runaway and SNL reproduce experimental tests performed on a Francis turbine at model scale designed by Andritz Hydro Canada Inc in the early 2000s. The measurements were performed at the Laboratory for Hydraulic Machines of École Polytechnique Fédérale de Lausanne in 2004. The Francis turbine studied has a specific speed at best efficiency point (BEP) of n_{QE}^=0.1 (definition in the IEC 60193 standard [16]). This turbine was composed of a spiral casing with 19 stay vanes, a distributor with 20 guide vanes and the runner with 15 blades. The guide vane opening at BEP is around 18°. The draft tube comprises a conical diffuser, a converging/diverging elbow and a trumpet diffuser.

The runaway condition was tested at the constant guide vane opening of α=31°. The head and the runner rotation speed were fixed at 11.2 m and 1000 rpm, respectively, to reach a zero torque condition. The SNL was tested under a fixed experimental head of 30 m and a fixed guide vane opening of α=1.5°. The runner rotation speed was imposed to reach the same speed factor n_{ED} (defined in the IEC 60193 standard [16]) as the prototype turbine operated at synchronous speed with the same guide vane opening. The runner produced a residual torque to overcome some losses in the turbine-generator assembly. At SNL, the runner produces 2% of the BEP torque, while the residual torque was negligible at runaway. The measurements at runaway and SNL were performed at σ_{Plant}.

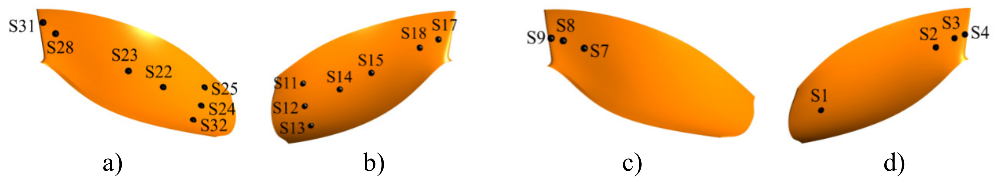

Figure 3. Pressure sensors a) blade 1 PS, b) blade 2 SS, c) blade 8 PS and d) blade 9 SS.

The average discharge, specific energy, runner rotation speed and static suction head H_s [m] were measured for each NL operating condition. Dynamic pressure measurements were performed with 18 miniature piezoresistive pressure sensors flush-mounted on four blades (blade 1 and blade 8 pressure side (PS) and blades 2 and 9 suction side (SS)) covering two hydraulic channels. The positions of the pressure sensors are shown in figure 3. The experimental technique and the measuring instruments are detailed in Nennemann et al. [17]. The pressure measurements were performed at a sampling rate of 20 kHz over 275 and 153 runner rotations at runaway and SNL, respectively. The resulting measurement uncertainty on the pressure measurements is evaluated at 0.5% for pressure values above the vapor pressure.

4. Numerical simulation of no-load conditions

4.1 Simulation strategies

The URANS equations are solved with the finite volume commercial solver ANSYS CFX 19.1. The Scale-Adaptive Simulation (SAS-SST) turbulence model is used for its capacity to resolve additional spectral content in unstable flows in comparison with standard RANS models [18].
Even if cavitation was present in the experiments, single-phase simulations were performed. To solve the URANS equations, the time-stepping algorithm uses an implicit second-order backward Euler scheme. The order of the upwind advection scheme for the momentum equations is defined via a blend factor β. A fix β of 0.95 was used to obtain close to second-order accurate solutions without significantly affecting the residual level on each velocity component. Kato-Launder production limiter and curvature correction were used.

The numerical simulations are performed on a domain composed of the distributor, runner and draft tube. The domain is shown in figure 4 a). In this domain, the rotation axis is Z aligned downward, in the turbine direction, while z=0 m is at the distributor's bottom. The spiral casing was only used in the preliminary simulations. For the final simulations, the velocity profiles and the turbulent quantities extracted from the simulations at runaway and SNL with the spiral casing were imposed at the distributor inlet. An extension with slip walls is used at the draft tube outlet to prevent backflow at the outlet boundary condition. Except for this extension, every other wall is treated with the no-slip condition.

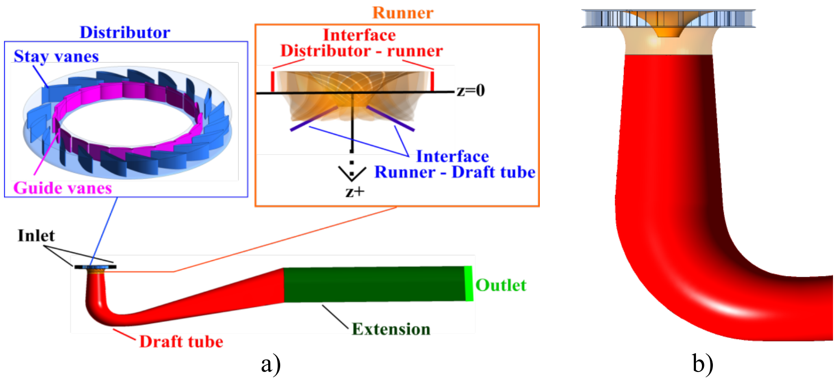

Figure 4. a) Numerical domain with a runner, b) Part of the hydraulic channel without a runner.

Transient rotor-stator interfaces are used to reproduce the complete interaction between the runner and the stationary components. A mass flow rate is imposed at the domain inlet at runaway based on the experimental measurements. Following Andritz's general practice, a turbulent intensity of 5% is imposed. A steady runner rotation speed is also imposed following the experimental measurements. An area-averaged static pressure calculated with the experimental suction head value H_s is imposed at the domain outlet.

Uncertainties in SNL measurements associated with the discharge evaluation and the guide vanes angles lead to using "tweaked" inflow conditions to represent the flow dynamics correctly. Hence, the guide vane opening and the discharge were chosen to match the experimental torque produced by the runner and the experimental head. This methodology should lead to similar experimental and numerical flow angles at the runner inlet and, according to equation (5), for the same ratio B_0/D_2, to similar RC_{u11} values. The rest of the setup is identical to the setup at runaway.

Runaway and SNL simulations use the ANSYS CFX scalable wall function. Time steps corresponding to (1/2)° of runner rotation or $8.33 \cdot 10^{-5}$s at runaway and (1/3)° of runner rotation or $5.97 \cdot 10^{-5}$s at SNL with five linear solver iterations are used. The RMS residuals always stay below $2.1 \cdot 10^{-5}$. The average Courant number is 1.10 at runaway and 1.06 at SNL. The maximum Courant number values, 12.00 at runaway and 10.45 at SNL, are near the draft tube outlet and in the extension.

Table 1 summarizes the mesh characteristics at runaway and SNL for each subdomain. An unstructured mesh is generated with an Andritz in-house tool for the stay vanes and the guide vanes. Structured meshes are used for the runner and the draft tube. The software Numeca AutoGrid5 is used for the runner mesh and ANSYS ICEM 18.1 is used for the draft tube mesh. An overview of the meshes has already been published in Fortin et al. [6].

Table 1. Mesh characteristics for the casing, the distributor (including the stay vanes), the runner and the draft tube at runaway and SNL.

	Casing	Distributor		Runner		Draft tube	
		Runaway	SNL	Runaway	SNL	Runaway	SNL
Number of nodes	2.7 M	5.8M	6.6M	12.2M	22.2M	3.0M	4.4M
Min angle	14°	34°	34°	29°	29°	20°	21.3°
Max AR	22	15	24	54	29	138	138
Max exp. Factor	21	5	11	54	2	138	3
y+	<100	<375	<325	<475	<400	<400	<400

Simulations with the same distributor, hub, shroud and draft tube as the runaway and the SNL simulations were also performed without runner blades. The channel formed by the hub and the shroud for those simulations is shown in figure 4 b). Those simulations were used to investigate the runner's effects on the swirl level and the velocity profile in the draft tube cone. Simulations without the runner follow the idea of Houde et al. [19]. The distributor and draft tube meshes in the simulations without the runner are the same as in the full-turbine simulations. The mesh in the channel formed by the hub and the shroud has similar element sizes as the runner mesh. The simulation strategy is exactly the same as in the full-turbine simulations. However, there is no rotating domain in the simulation without runner blades.

4.2 Validation of the numerical simulations

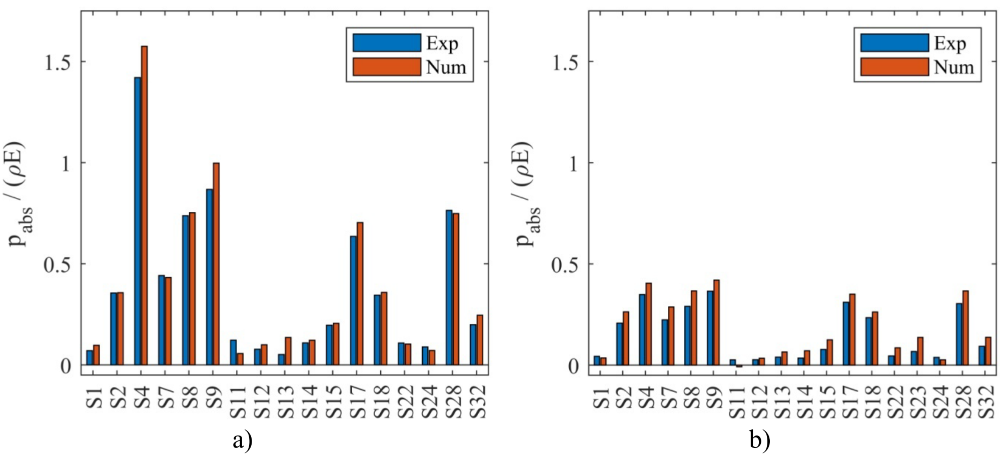

Figure 5. Comparison of average experimental and numerical absolute pressures normalized by ρE for a) runaway and b) SNL.

The numerical strategy was validated by comparing the average experimental and numerical unsteady absolute pressures over the runner blades when the simulations reached a stabilized condition with pressure levels having constant averaged values. At runaway, the numerical values are calculated using 45 runner rotations of the stabilized solutions, while for SNL, 15.2 rotations were used. Figure 5 compares the average experimental and numerical pressure ($p_{abs}/\rho E$) at the pressure sensors locations described in section 3 for the runaway in a) and the SNL in b). The experimental and numerical normalized pressures have absolute differences below 0.15 $p_{abs}/\rho E$ for the runaway and 0.08 $p_{abs}/\rho E$ for the SNL. Overall, those results indicate that the simulation strategies accurately predict the average pressure distribution over the blades at runaway and SNL and, consequently, provide a good prediction of the average runaway and SNL conditions.

Several error sources may explain the small deviations between the experimental and numerical results: the differences between the test conditions and the boundary conditions; the geometrical differences between the experimental and the numerical models; the turbulence modeling; the omission of the cavitation effects in the simulations; the finite size of the pressure sensors (3 mm) in the laboratory in contrast to the point extraction process in the simulations.

5. Analyses

5.1 Flow topology in the draft tube cone at runaway and SNL

This paper focuses on the swirl level at three sections (A, B and C) shown in figure 6 a). Section A is located at the runner inlet, at the interface between the distributor and the runner. Section B follows approximately the shape of the blade trailing edges and is located at the interface between the runner and the draft tube. Section C is located at z=D_2.

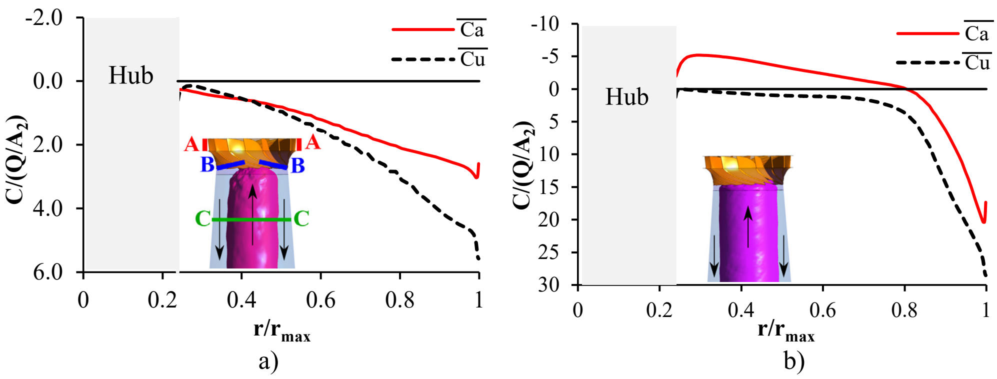

Figure 6. Variation of $\overline{C_a}$ and $\overline{C_u}$ with r/r_{max} at Section B at a) runaway and b) SNL.

Figure 6 shows the normalized average axial velocity ($\overline{C_a}/(Q/A_2)$) and circumferential velocity ($\overline{C_u}/(Q/A_2)$ as a function of the normalized radius r/r_{max} at Section B at runaway in a) and SNL in b). The radius r_{max} [m] is the maximum radius of the plane. Figure 6 also shows the average outer limit of the backflow in the draft tube in pink at runaway in a) and SNL in b). The average flow topologies at runaway and SNL in the draft tube are different. On average, the backflow does not enter the runner outlet at runaway since the values of $\overline{C_a}$ are always positive (figure 6 a)). At SNL, figure 6 b) clearly shows that the backflow enters the runner outlet. The average backflow, where $\overline{C_a}$ is negative, covers 81% of the runner outlet area. At runaway, $\overline{C_u}$ increases from the hub to the shroud (figure 6 a)). At SNL, $\overline{C_u}$ stays low in the backflow core and increases significantly from the backflow outer limit to the shroud (figure 6 b)).

5.2 RC_{u11}

5.2.1 Numerical values of RC_{u11}

Table 2. RC_{u11} calculated at Section A and Section B at runaway and SNL for domains with and without the runner blades.

	With runner blades		Without runner blades	
	Runaway	**SNL**	**Runaway**	**SNL**
Section A	2.03	43.10	2.03	43.03
Section B	2.03	33.68	1.98	34.87

Table 2 compares RC_{u11} at Section A and Section B at runaway and SNL (data "With runner blades"). RC_{u11} has been calculated at each timestep to consider the fluctuating terms. The average of all RC_{u11} values is presented in table 2. According to equation (3), for a perfect NL condition (T_{Eu}=0 Nm, when the friction losses are negligible), RC_{u11} is equal at the runner inlet and outlet or at Section A and Section B. The runaway condition produces a negligible residual torque with a high discharge. For this reason, the Euler torque parameter has a negligible value and RC_{u11} at Section A and Section B are the same (RC_{u11}=2.03). At SNL, 2% of the torque at BEP is still produced by the runner with a very low discharge. Consequently, the Euler torque parameter is non zero and RC_{u11} at Section A and Section B are not exactly the same. Indeed, the Euler torque parameter is $(T_{Eu}D_2)/(\rho Q^2)$=9.25 while RC_{u11} at Section A and Section B are different by 9.42. Those values are similar but not strictly identical because of the numerical uncertainties and the convergence level of the numerical averages.

5.2.2 Comparison of RC_{u11} and the velocity profiles in channels with and without a runner. Table 2 shows the average values of RC_{u11} at Section A and Section B in the domains without the runner blades. The sections are located at the same place in the domains with and without the runner blades. RC_{u11} at the runner inlet (Section A) are the same for the domains with and without the blades at runaway and SNL considering the numerical uncertainties. Indeed, RC_{u11} are exactly 2.03 at runaway and RC_{u11} are different by less than 1% at SNL. The runner does not influence the swirl level at the guide vane outlet. The analytical equation (5) indicates that the flow angle (dictated by the guide vane opening) and the ratio B_0/D_2 control the swirl level. The simulations with and without the runner have the same B_0/D_2 and the same guide vanes at the same opening.

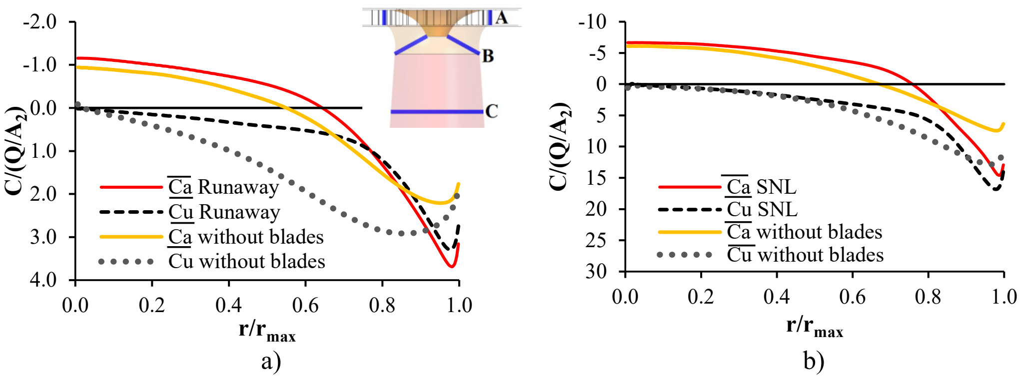

Figure 7. Variation of $\overline{C_a}$ and $\overline{C_u}$ with the normalized radius r/r_{max} at Section C at a) runaway and b) SNL, including the simulation results without runner blades.

Without the runner, RC_{u11} at Section B is lower than at Section A because of the moment produced by the viscous forces on the hub and shroud walls. In other words, the Euler torque parameter in equation (3) is non-zero. However, RC_{u11} at Section B for the simulations with and without the runner blades at runaway and SNL are quite similar. At Section B, RC_{u11} at runaway is 2.03 with the runner and 1.98 without the runner. At SNL, RC_{u11} at Section B is 33.68 with the runner and 34.87 without the runner. Comparing the simulations with and without the runner illustrates the runner's impact on the flow in the draft tube cone at NL conditions.

Figure 7 shows $\overline{C_a}$ and $\overline{C_u}$ as a function of the normalized radius r/r_{max} at Section C at runaway in a) and SNL in b), including the simulation results without runner blades. The backflow is not only caused by the runner since the simulations without blades have negative values of $\overline{C_a}$ at Section C. The simulations of Houde et al.[19] lead to the same conclusion for an axial turbine. However, the backflow size is different in the draft tube when a runner is in the hydraulic channel. At runaway, the backflow outer diameter is r/r_{max}=0.66 with the runner blades and r/r_{max}=0.55 without the runner blades at Section C. The average discharge in the backflow core, where $\overline{C_a}$ is negative, normalized to the total discharge in the turbine is $Q_{Backflow}/Q_{Total}$ = -0.31 with the blades and $Q_{Backflow}/Q_{Total}$ = -0.18 without the blades. At SNL, the backflow outer diameter is r/r_{max}=0.77 with the blades and r/r_{max}=0.67 without the blades at Section C. The normalized discharge in the backflow core is $Q_{Backflow}/Q_{Total}$ = -2.80 with the blades and $Q_{Backflow}/Q_{Total}$ = -1.77 without the blades.

Figure 8 shows the average streamlines projected onto a conformal plane at a blade span of 0.9 at runaway in a) and SNL in b). A blade span of 0 is at the hub and a blade span of 1 is at the shroud. The blade trailing edge at a blade span of 0.9 intersects Section B at r/r_{max}=0.92. The blade trailing edges are thus outside the backflow at a span of 0.9 at runaway and SNL. According to the projected streamlines near the runner outlet, the relative flow angle appears to follow the blade geometry at runaway (figure 8 a)) while, at SNL (figure 8 b)), the flow more or less follows the blade angle in the area with a positive flow (in the turbine direction). Thus, for a given RC_{u11}, the blades influence the relative flow direction at the runner outlet.

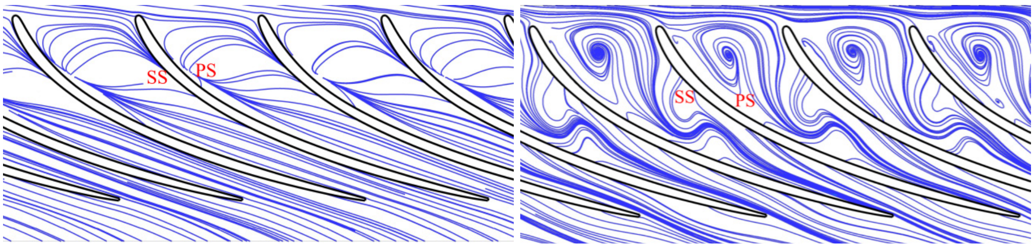

Figure 8. Average streamlines projected onto a conformal plane at a blade span of 0.9 at a) runaway and b) SNL.

5.2.3 Validation of the analytical formulation of RC_{u11}. Equation (5) proposes an analytical formulation of RC_{u11} as a function of geometrical parameters (B_0/D_2) and the flow angle at the guide vane outlet. Table 3 shows the value of α and θ in the numerical simulations at runaway and SNL and the resulting $(RC_{u11})_1$ using those values in equation (5). At runaway, $(RC_{u11})_1$ calculated at Section A with the analytical equation (5) is 10% higher than $(RC_{u11})_1$ calculated with equation (4) (see table 2). At SNL, the difference between $(RC_{u11})_1$ calculated with equation (5) and equation (4) (see table 2) is less than 1%. Equation (5) predicts the right order of magnitude of $(RC_{u11})_1$ for the two NL conditions.

Table 3. Guide vane opening angle α, average flow correction angle θ and RC_{u11} at Section A.

	α	**θ**	**$(RC_{u11})_1$**
Runaway	31°	-8.8°	2.23
SNL	2.3°	-1.1°	43.03

At runaway, the area average value of θ at every timestep averaged over all timesteps is θ=-8.8°, while θ calculated with the time average velocity components only is θ=-11.7°. This example illustrates the importance of fluctuating terms. The instantaneous velocity components C_u and C_m can be decomposed into average parts $\overline{C_u}$ and $\overline{C_m}$ and fluctuating parts C_u' and C_m' caused by turbulence, structured hydraulic phenomena or periodic perturbations. The average of each fluctuating velocity component is zero ($\overline{C'_u}$=0 m/s, $\overline{C'_m}$=0 m/s), but the average of the multiplication or the division of two fluctuating velocity components ($\overline{C'_{m1}/C'_{u1}}$, $\overline{C'_u C'_a}$) is non-zero. If the fluctuating velocity components are non-negligible, like in the small vaneless space at runaway, the formulation $\bar{\theta}=\tan\left(\overline{\frac{C_{m1}+C'_{m1}}{C_{u1}+C'_{u1}}}\right)$-α is not equal to the formulation $\bar{\theta}=\tan\left(\frac{\overline{C_{m1}}}{\overline{C_{u1}}}\right)$-α. Consequently, RC_{u11} should ideally be evaluated from unsteady simulations and not steady RANS simulations to consider the fluctuating terms. At SNL, where the vaneless space is larger, the evaluation of θ with the average velocity components is accurate with θ=-1.1°.

5.3 Comparison between RC_{u11} and the Swirl number

Table 4. Comparison between RC_{u11} and the Swirl number at Section B and Section C at runaway and SNL.

	RC_{u11}		**S**	
	Runaway	SNL	Runaway	SNL
Section B	2.03	33.68	1.29	1.09
Section C	1.97	33.50	0.73	0.72

Table 4 compares the average value of RC_{u11} and the Swirl number calculated at Section B and Section C at runaway and SNL. While RC_{u11} clearly shows a swirl increase between runaway and SNL, the Swirl number has the same magnitude between those NL conditions. At Section B, the value of the Swirl number is even lower at SNL than at runaway. At Section C, the value of the Swirl number is quasi identical between the two NL conditions.

For a plane perpendicular to the flow in the draft tube cone, the Swirl number takes a form commonly used in the literature [9], [13]:

$$S_{DT\ cone}=\frac{\int_0^R r^2 C_u \cdot C_a dr}{(D_2/2)\int_0^R r C_a^2\, dr}. \tag{8}$$

In equation (8), R [m] is the maximum radius of the plane where the swirl is evaluated. Figure 9 compares the terms inside the integrals of equation (8). Those terms are normalized by EA_2: $r^2C_uC_a/(EA_2)$, $(D_2/2)(rC_a^2)/(EA_2)$. At a radius of r/r_{max}=0, $r^2C_uC_a$ and $(D_2/2)(rC_a^2)$ are necessarily equal to zero. At the backflow outer limit, $\overline{C_a}$ is zero and $r^2C_uC_a$ and $(D_2/2)(rC_a^2)$ are also equal to zero. From the radius r/r_{max}=0 to the backflow outer radius ($\overline{C_a}$ =0 m/s), $r^2C_uC_a$ and $(D_2/2)$ (rC_a^2) values stay low, around zero. Consequently, the swirl main contributing velocities come in the positive flow area, outside the backflow.

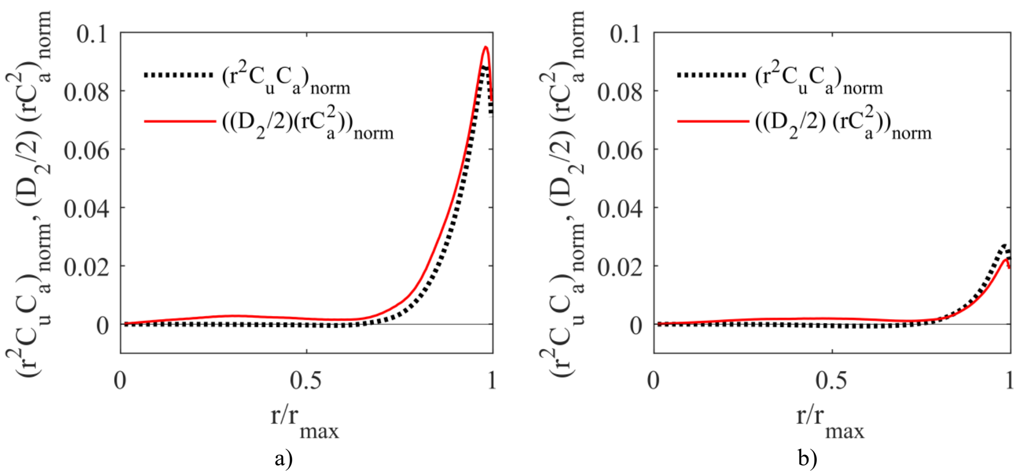

Figure 9. $r^2C_uC_a/(EA_2)$ and $(D_2/2)(rC_a^2)/(EA_2)$ as a function of r/r_{max} at Section C at a) runaway and b) SNL.

The discharge in the positive flow area is the sum of the total discharge in the turbine and the discharge brought up by the backflow. The positive flow area is only a portion of the total area at Section C. Consequently, $\overline{C_a}$ reaches average values much higher in the positive flow area than the theoretical value $C_a=Q/A_{Section\ C}$. The highest values of $\overline{C_a}$ are reached at a large radius. Thus, $(D_2/2)(rC_a^2)$ at NL reaches high values contributing to lower the value of the Swirl number. The magnitude of $(D_2/2)(rC_a^2)$ depends on the backflow diameter and the negative discharge brought up into the turbine by the backflow. Since the backflow characteristics are related to the swirl level at the runner outlet [1], [4], [5], the magnitude of $(D_2/2)(rC_a^2)$ depends on the swirl level. In the Swirl number equation, the numerator and the denominator depend on the swirl level and vary in the same way with the backflow size. Thus, the Swirl number cannot reflect the change of flow topology in the draft tube as a function of the swirl level at NL.

6. Conclusion

This paper studies the average runaway and SNL conditions and the flow topology in the draft tube cone related to the swirl level in the turbine. Numerical data from URANS simulations with a SAS SST turbulence model were used. The ability of the numerical methodology to predict the average NL conditions is validated against experimental pressure measurements in the runner. The main conclusions of the paper are:

- RC_{u11} is conserved at the runner inlet and outlet for a perfect NL condition.
- RC_{u11} is only dependent on the flow angle at the guide vane outlet, the distributor height and the runner outlet diameter.
- The Swirl number cannot be used at NL conditions to classify the flow as a function of the swirl level as done previously for the part load operation [9]. The numerator and the denominator in the Swirl number definition (equation (6)) vary in the same direction and with similar magnitude depending on the swirl level. It is a direct consequence of the large backflow under the runner. The difference between the Swirl number at runaway and SNL is not representative of the difference of flow topology in the draft tube cone.

References

[1] Fortin M, Nennemann B, Deschênes C, and Houde S, 2022, Classification of the hydraulic behavior along the no-load curve of Francis turbines, *ASME J. Fluids Eng.*, **144**, no. 3, p. 031205 , doi: https://doi.org/10.1115/1.4051895.

[2] Nicolle J, Morissette J F, and Giroux A M, 2012, Transient CFD simulation of a Francis turbine startup, *IOP Conf. Ser. Earth Environ. Sci.*, **15**, p. 062014.

[3] Mende C, Weber W, and Seidel U, 2016, Progress in load prediction for speed-no-load operation in Francis turbines, *IOP Conf. Ser. Earth Environ. Sci.*, **49**, p. 062017.

[4] Skotak A, 1996, Modelling of the swirl flow in a Kaplan turbine operating under off-cam conditions, *Modelling, testing & monitoring for hydro powerplants*, (Lausanne, Switzerland), pp. 197–204. doi: 0952264234.

[5] Bettocchi R, Cantore G, Magri L, and Ubaldi M, 1982, Analyse expérimentale de l'écoulement dans la zone axiale des canaux adducteurs des turbines-hélices, *Houille Blanche*, **37**, no. 7–8, pp. 599–606, doi: 10.1051/lhb/1982046.

[6] Fortin M, Nennemann B, Houde S, and Deschênes C, 2019, Numerical study of the flow dynamics at no-load operation for a high head Francis turbine at model scale, *IOP Conf. Ser. Earth Environ. Sci.*, **240**, p. 022023.

[7] Dörfler P, Sick M, and Coutu A, 2012, Flow-Induced Pulsation and Vibration in Hydroelectric Machinery: Engineer's Guidebook for Planning, Design and Troubleshooting. *Springer*.

[8] Jacob T, 1993, Evaluation sur modèle réduit et prédiction de la stabilité de fonctionnement des turbines Francis, Thesis (PhD), *École polytechnique fédérale de Lausanne*,(Switzerland).

[9] Favrel A, Gomes Pereira Junior J, Landry C, Müller A, Nicolet C, and Avellan F, 2018, New insight in Francis turbine cavitation vortex rope: role of the runner outlet flow swirl number, *J. Hydraul. Res.*, **56**, no. 3, pp. 367–379.

[10] Cassidy J J, 1969, Experimental study and analysis of draft-tube surging, U.S. *Department of the Interior, Bureau of Reclamation*, Denver, (Colorado), HYD-591.

[11] Wahl T L 1990 Draft tube surging hydraulic model study, Thesis MSc, *Colorado State University*, (Fort Collins, Colorado), 1990.

[12] Fortin M, Nennemann B, Deschênes C, and Houde S, 2021, Evolution of discharge and runner rotation speed along no-load curves of Francis turbines, *IOP Conf. Ser. Earth Environ. Sci.*, **774**, no. 1, p. 012121, doi: 10.1088/1755-1315/774/1/012121.

[13] Susan-Resiga R, Dan Ciocan G, Anton I, and Avellan F, 2005, Analysis of the Swirling Flow Downstream a Francis Turbine Runner, *ASME J. Fluids Eng.*, **128**, pp. 177–189.

[14] Gupta A K, Lilley D G, and Syred N, 1984, Swirl flows, *Energy and engineering science series*, Tunbridge wells, (England: ABACUS PRESS).

[15] Vignat G, Durox D, and Candel S, 2022, The suitability of different swirl number definitions for describing swirl flows: Accurate, common and (over-) simplified formulations," Prog. *Energy Combust. Sci.*, **89**, p. 100969, doi: 10.1016/j.pecs.2021.100969.

[16] IEC 60193, 2019, Hydraulic turbines, storage pumps and pump-turbines - Model acceptance tests. *International Electrotechnical Commission*.

[17] Nennemann B, Vu T C, and Farhat M, 2005, CFD prediction of unsteady wicket gate-runner interaction in Francis turbines: A new standard hydraulic design procedure, *HYDRO 2005*, (Austria).

[18] Nennemann B, Morissette J F, Chamberland-Lauzon J, Monette C, Braun O, Melot M, Coutu A, Nicolle J and Giroux A M, 2014, Challenges in Dynamic Pressure and Stress Predictions at No-Load Operation in Hydraulic Turbines, *IOP Conf. Ser. Earth Environ. Sci.*, **22**, p. 032055.

[19] Houde S 2018 Analysis of the part load and speed-no-load flow dynamics in a model propeller hydraulic turbine, Ph.D. thesis, *Laval University (Canada)*.